Journal of Petroleum Science and Technology 11(3): 31, 2021, Pages 11-23
DOI:10.22078/JPST.2021.4480.1726

Journal of Petroleum Science and Technology

https://jpst.ripi.ir/

Characterization of the Amount of Swept and Unswept Fractions Between Two Wells in the Presence of Reservoir Anisotropy

Karim Karami, Mohsen Masihi *and Hossein Barati

Department of Chemical and Petroleum Engineering, Sharif University of Technology, Tehran, Iran

Abstract

The reservoir heterogeneity controls interwell connectivity and affects reservoir dynamics. An approach is to use continuum percolation to study the flow behavior of low to intermediate net-to-gross reservoirs. In this study, reservoir models with a permeability contrast have been used, and the interwell connectivity between two wells and the remaining unswept oil has been determined. The percolation parameters, including the amount of recoverable oil connected between two wells and the amount of unswept oil (also referred to as dangling end fraction (that control fluid displacement (e.g. waterflooding) vary as a function of sand body size and reservoir size. These properties show a power-law function of net-to-gross (i.e. occupation fraction) with some exponents called critical exponents. There exist a few publications on the numerical values of these parameters. The main contribution of this study is to investigate the effects of reservoir anisotropy on the percolation parameters. To determine the swept (backbone) fraction connected between two wells, the flow-based criteria depending on the system size have been proposed. The results show that the critical exponents for the backbone and dangling ends are in the range of 0.3to 0.45 and -0.45 to -0.20. It is notified that the limitation to perform simulations on infinite systems results in a range for these exponents, although there exist unique values for infinite systems. Moreover, a sensitivity analysis is implemented to find the correct flow-based criteria for the backbone. The results of this study extend the applicability of the percolation properties curves for anisotropic reservoirs.

Keywords: Continuum Percolation, Heterogeneity, Reservoir Connectivity, Backbone, Dangling Ends, Anisotropy.

Introduction

The structures of porous media are affected by the complex depositional process, which sometimes results in high-permeability sands and low-permeability shales, mudstone and siltstone. In such geometrically complex systems with a given spatial distribution of sand bodies, the flow behavior depends not only on the quality of the sand bodies but also on their connectivity [1, 2]. Applications of such systems with significant permeability contrast may be found in hydrology, e.g. solute transport, oil and gas reservoirs, e.g. waterflooding, geothermal reservoirs and wastewater disposal [3-6].

Connectivity and conductivity are the main issues in geometrically complex mediums. In this study, by connectivity, a static connection of permeable regions (or a specific rock type) distributed in a given reservoir is meant by us. Also, conductivity refers to the dynamic behavior of such mediums, e.g. effective permeability of the medium. For example, such connectivity has an indisputable effect on the flow behavior in reservoirs. One conventional approach to assess the impact of such connectivity is to generate many realizations (i.e. equiprobable reservoir models) and to perform numerical flow simulations that are very time-consuming.

On the other hand, percolation theory, initially developed for infinite systems, provides a suitable statistical approach to investigate connectivity and conductivity in heterogeneous systems [3, 4]. Also, finite-size scaling within percolation theory has been applied to deal with the boundary effects in finite size systems [4]. There are a variety of percolation types, i.e. bond/site percolation (on fixed bonds/points, respectively) and continuum percolation (by letting the objects overlap) [7]. The flexibility of the continuum percolation framework enabled it to be suitable for evaluating the connectivity and conductivity of heterogamous media [2, 7, 8].

**Corresponding author:* Mohsen Masihi, Department of Chemical and Petroleum Engineering, Sharif University of Technology, Tehran, Iran

E-mail addresses: masihi@sharif.edu

Received 2021-05-08, Received in revised form 2021-10-28, Accepted 2021-11-24, Available online 2022-05-15.

In 1957, Broadbent and Hammersley first explored percolation theory [9], and since then, it has been developed in both applications and variety [8, 10]. For example, the connectivity and conductivity of a 2D porous media made of randomly overlapping sand bodies distributed in impermeable background rock were investigated by King in 1990 [1]. It has been emphasized the existence of a specific percolation threshold above which the connectivity of the system increases rapidly [1]. In 1992, randomly, distributed spheres and circles as permeable units, respectively in 2D and 3D were used by Berkowitz and Balberg, and it was shown that the power laws with unique parameters could be applied to predict the hydraulic conductivity of the systems [11].
Moreover, in 1995, Berkowitz studied the fracture networks and proposed a minimum number of intersections per fracture and defined the probability that any fracture is connected to the spanning cluster to evaluate the connectivity [12]. The threshold for randomly spatially spheres distributed in a large scale 3D continuum system was estimated by Rintoul and Torquato in 1997, and the power-law exponents were calculated [13]. The reported algorithms, among the others, to determine the percolation sub-networks include Hoshen et al. (1997) for the connected cluster (which connects both sides of the systems through permeable objects) and internal perimeters of the clusters or Dokholyan et al. (1998) for the minimal path (or chemical distance) between two sites, defined as shortest path on a percolating cluster connecting the two sites [14,15]. Other publications discuss the universality of the percolation exponents [16-19].
The extensions of basic percolation are to include the effects of anisotropy in the finite-size scaling framework [2, 20], the spatial correlation which may modify the power-law exponents [21], and the object sizes which may be replaced by an effective length within the finite size analysis [22, 23]. However, in the case of a very broad size distribution, the percolation exponents may deviate from their universal values [24]. Another extension uses the point-to-point connection in 2D problems instead of conventional line-to-line connection. In 2016, point-to-point connection criteria for continuum percolation problems were used by Tavagh-Mohammadi et al. [25] and Sadeghnejad and Masihi [26], and the percolation critical exponents were determined.
Several researchers have reported the applications of percolation approach to geoscience problems. In 2001, the breakthrough time of an injected fluid between a pair of injection and production wells from the percolation approach was estimated by King et al [27] and compared with the conventional flow simulations. In 2006, facies connectivity in a reservoir made of isotropic and anisotropic facies was modeled by Nurafza et al. [28]. In 2011, the average reservoir conductivity of Norouz oil field, Iran, was obtained by Sadeghnejad et al. from both percolation approach and conventional numerical modeling simulation [23]. In 2014, continuum percolation was used to obtain volumes of oil recovered from the backbone and the remained oil in dangling ends by Wen et al. [29].
In this study, on the connectivity, backbone and dangling end fractions in 2D reservoir models with anisotropic sand bodies distributed randomly within the model are concentrated by us. This study will focus on the correct determination of backbone and dangling end fractions in anisotropic reservoirs using percolation finite-size scaling law of percolation theory. Furthermore, a sensitivity analysis on percolation threshold for determining a minimum flow threshold is proposed

Materials and Methods

Continuum percolation deals with models in which permeable objects (high permeability regions) are distributed randomly in the system, and there is a chance of overlapping. An example related to oil and gas reservoir by which we discuss its theoretical background is a system made of overlapping high permeability sand bodies distributed randomly in an impermeable background. We define occupancy probability, p, (equivalent to net-to-gross in reservoir studies) as the area fraction (or volume fraction in 3D) of a system occupied by the sand bodies. At each p value, there will be a number of clusters made by sand bodies in the system. There is also a specific p called percolation threshold, P_c^{∞}, at which a spanning cluster (i.e. connected cluster) appears, and above it, there is global connectivity within the medium through the sand bodies.
The strength of this connected cluster can be described by a percolation parameter called percolation probability, P, which is defined as the probability that a site belongs to the connected cluster. The connected cluster (also called spanning cluster) can then be divided into backbones (those parts which carry the main flow) and dangling ends (those parts which have a negligible contribution to the flow). For a very large system size (infinite), these three percolation parameters follow a similar power law, i.e. [4,10],

$$P(p) \propto (p - p_c^{\infty})^{\beta} \quad (1)$$

$$B(p) \propto (p - p_c^{\infty})^{\beta_B} \quad (2)$$

$$D(p) \propto (p - p_c^{\infty})^{\beta_D} \quad (3)$$

where β, β_B and β_D are the critical exponents for the connected fraction, backbones and dangling end fractions, respectively, and p is the occupancy probability (i.e. net to gross in reservoir studies). The numerical values for β, β_B and β_D are given in Table 1.

Table 1. The numerical values for the critical exponents

Critical exponents	2D	3D	Reference
β		0.41	[7,8]
β_B	0.475	1.05	[4,7]
β_D	-0.423	-	[4]
v	0.75	0.88	[7,8]

However, in reality, all the systems are finite. There is a finite-size dependency for percolation parameters. For example, an apparent percolation threshold can be defined for the finite-size systems as [4, 10],

$$\tilde{P}_c(L) - p_c^{\infty} \propto L^{\frac{-1}{\nu}} \tag{4}$$

where $\tilde{P}_c$ is the apparent percolation threshold, and v is the correlation length exponent. Moreover, the connected fraction P, backbones B and dangling ends D fractions have the following finite-size dependency,

$$P(p,L) = L^{-\beta/\nu}\Im\left[(p-p_c^{\infty})L^{1/\nu}\right] \tag{5}$$

$$B(p,L) = L^{-\beta_B/\nu}\Im_B\left[(p-p_c^{\infty})L^{1/\nu}\right] \tag{6}$$

$$D(p,L) = L^{-\beta_D/\nu}\Im_D\left[(p-p_c^{\infty})L^{1/\nu}\right] \tag{7}$$

where $\Im$, $\Im_B$ and $\Im_D$ represent type curves for the P, B and D, respectively that can be determined from numerical simulations.

It must be emphasized that the percolation parameters used in Equations 5 to 7 are the respectively mean connected fraction, mean backbones and mean dangling ends fractions obtained over all possible realizations of the reservoir models. Similarly, the errors (represented statistically by standard deviation) on the mean values of these percolation parameters (which is shown by Δ(p,L)) can be determined which also have a similar finite-size behavior, i.e.,

$$\Delta(p,L) = L^{-\beta/\nu}\Re\left[(p-p_c^{\infty})L^{1/\nu}\right] \tag{8-1}$$

$$\Delta_B(p,L) = L^{-\beta_B/\nu}\Re_B\left[(p-p_c^{\infty})L^{1/\nu}\right] \tag{8-2}$$

$$\Delta_D(p,L) = L^{-\beta_D/\nu}\Re_B\left[(p-p_c^{\infty})L^{1/\nu}\right] \tag{8-3}$$

However, reservoir models themselves or sand bodies are often not isotropic, so Equations 5 to 8 may not be used straightforwardly to such reservoirs.

A practically relevant feature that should be considered in percolation approach is the effect of anisotropy. Anisotropy may be implemented by considering different lengths of the sand bodies in the X and Y directions. Hence, in such cases, an aspect ratio can be defined as:

$$\omega = \frac{L_X}{L_Y} \tag{9}$$

where L_X and L_Y are the lengths of the sand bodies in the X and Y directions. If there is a distribution for sandbody lengths, an effective sand body size for the whole system can be introduced to define this aspect ratio [4,12]. As shown and validated previously by Masihi et al. [20] and Sadeghnejad et al. [2], for the case of connectivity and permeability properties, the scaling relations (Equation 8) may be applied to anisotropic systems provided by us; moreover, we use an anisotropic apparent percolation threshold $\tilde{p}_c$ (defined below) and multiply the term $\omega^{1/2}$ in the right-hand side of Equation 8, as obtained by the following equation (Equation 10).

$$\tilde{p}_c - p_c^{\infty} = \Lambda_i(\omega)L_x^{-1/\nu} \tag{10}$$

where i indicates the X or Y directions and the coefficient to be determined numerically. The reason for proposing the geometric mean length $\omega^{1/2}=(L_x L_y)^{1/2}$ is due to the dependency of variance in connectivity on the mean cluster size in the system [4]. This paper uses a similar approach to Masihi et al. [20] and Sadeghnejad et al. [2] to account for the anisotropy in the backbone and dangling ends fractions properties.

Models Description

Imagine a squared 2D medium with a side size of L within which the sand bodies with size $a \times b$ are distributed randomly. A MatLab code has been developed to perform the simulations, and the statistics have been summarized. The framework and details of how the base code for isotropic systems works can be found in References [2,4,20]. Isotropy existed when a=b. To calculate the percolation parameters p, P, B and D, a fine grid of size 1/10 of the sand bodies has been covered by us. Also, appropriate algorithms are needed to determine the connected cluster and the backbone and dangling ends fractions. In this study, the Hoshen algorithm was used to define the connected cluster [30] and a flow-based algorithm [4, 29] to characterize the backbone and dangling ends fractions.

In Figure 1, realizations of overlapping squared sand bodies of side size 10 within a system of size L=100 at various densities of sand bodies (a) p=0.15, p=0.3, (c) p=0.45, (d) p=0.6, (e) p=0.75 and (f) p=0.9 are shown. Moreover, in Figure 2, various clusters (in different colors) that existed in realizations given in Figure 1 are shown. As expected, not all parts of these clusters contribute to the main flow through the system. Hence, it is necessary to characterize those parts of connected clusters which carry the main flow. To do this, first, the isolated clusters must be removed as they have no contribution to the main flow.

Then, to determine the backbone fraction or those parts of connected clusters which carry the main flow, single phase flow for an incompressible fluid is solved to determine the pressure distribution with the governing equation,

$$\nabla K.\nabla P = 0 \tag{2}$$

where K is the permeability, and P is the pressure field. From this, then, the Darcy law can be used to calculate the total flow in the system and the flow in both the X and the Y directions for each grid cell. As emphasized by Wen et al. in 2014 [29], a minimum flow threshold may be set to characterize the backbone fraction. If the fluid ratio that passes through a grid cell to the total fluid inside the medium is greater than this preset threshold, then it belongs to the backbone of the connected cluster. Otherwise, it belongs to the dangling ends. However, in practice, the method of choosing this threshold is a challenge. For example, a threshold of 5% for the ratio of grid flow to the total flow without any justification was used by Wen et al. in 2014 [29]. The question raised is that this threshold may depend on the system size and net to gross p. In this study, four criteria to set the threshold are proposed for the first time, as summarized in Table 2. In the proposed approach, the threshold by perpendicular area to the flow to consider the effect of the system size is normalized. As the system gets larger, the amount of total flow will increase. Hence, perpendicular area to the flow is used to eliminate the effect of system size on the total flow. After the backbone fraction has been determined, the dangling ends can be obtained by:

$$P = B + D \tag{12}$$

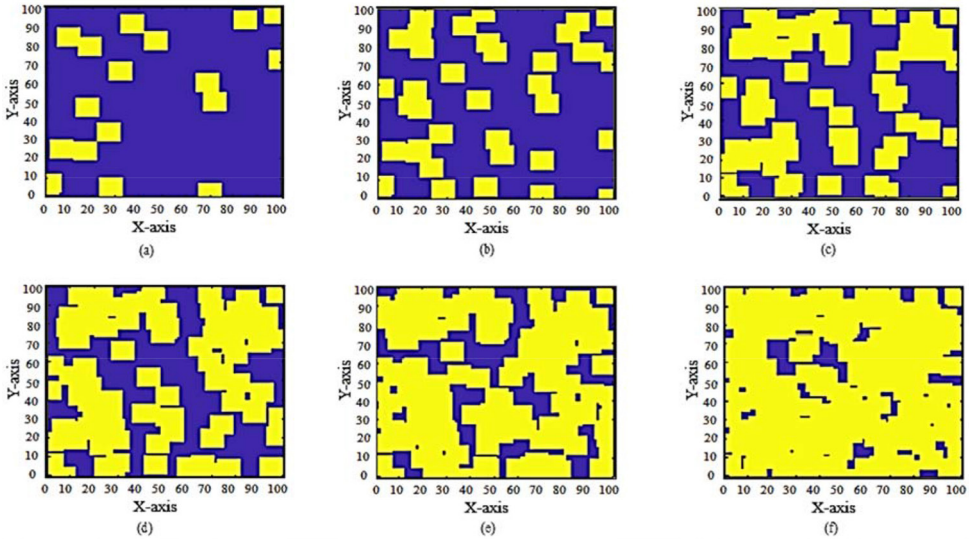

Fig. 1 Continuum percolation for a system size of L=10 and sand body size of 10×10 at various p values, the darker color represents the impermeable background, and the light one represents the sand bodies. (a) p=0.15, (b) p=0.30, (c) p=0.45, (d) p=0.60, (e) p=0.75 and (f) p=0.90.

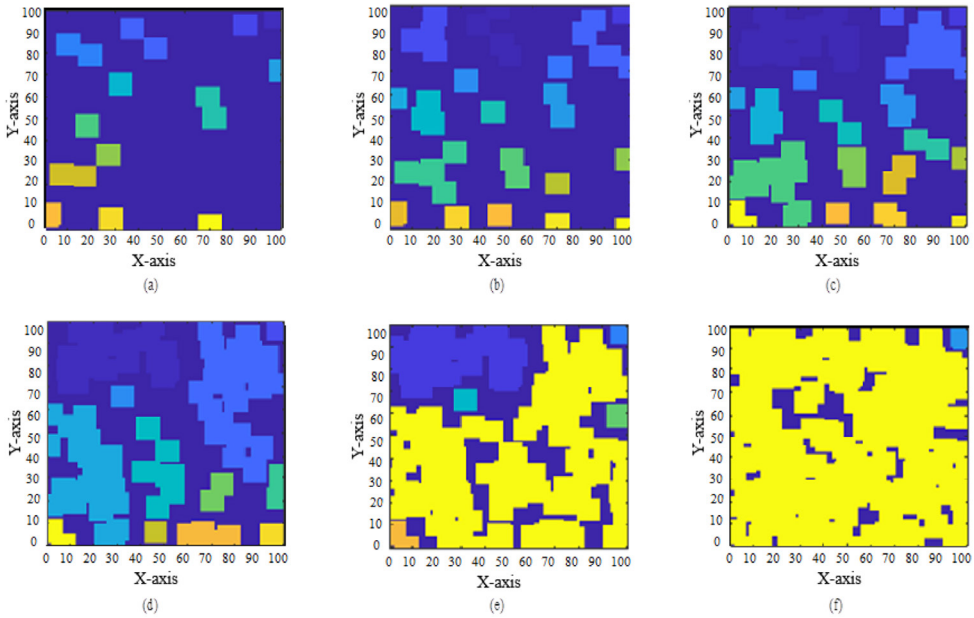

Fig. 2 Illustration of various clusters shown in different colors in the realizations shown in Figure 1, (a) p=0.15, (b) p=0.30, (c) p=0.45, (d) p=0.60, (e) p=0.75 and (f) p=0.90.

Table 2 Criteria for choosing the flow threshold that is used in determining the backbone and dangling ends fraction ("Ac" refers to the perpendicular area to the flow).

Criteria No.	Flow Threshold = % of the total flow
1	$\frac{1}{Ac}\times 100$
2	$\frac{3}{4}\frac{1}{Ac}\times 100$
3	$\frac{1}{2}\frac{1}{Ac}\times 100$
4	$\frac{1}{4}\frac{1}{Ac}\times 100$

where B and D represent the backbone and dangling ends fraction respectively. As an illustrative example, Figure 2 (e) shows a percolated system with a spanning cluster shown in yellow. If four different flow thresholds criteria listed in Table 2 are applied to this (Figure 2 e), different backbone structures may be obtained, as shown in Figure 3. This emphasized that if a smaller flow threshold is considered, the strength of the backbone fraction increases and the dangling ends fraction decreases. After sensitivity analysis on the flow threshold, No. 3 is used to distinguish the backbone from the dangling ends fraction.

After the developed code in Matlab has been run, the occupancy probability, percolation probability, percolation threshold, backbone, and dangling ends fractions have been determined.

These statistics for all the generated realizations have to be collected, and then the average values of each parameter and their standard deviations were determined. However, as in other similar simulation studies, to ensure that the collected data are statistically reasonable, a minimum number of realizations for each system size must be considered. The sensitivity analysis on a controlling parameter like the percolation threshold must be determined.

In all generated models, the sand body size is considered to fix with size 10x10. Six different system sizes from 50x50 to 500x500 have been used to build isotropic models (where the aspect ratio ω=1). To build anisotropic models, 10 different models with a range of aspect ratios described in Table 3 are considered.

Results and Discussion

The results collected from both isotropic and anisotropic models are presented in this section.

Isotropic Sandbody Models

Six different system sizes ranging from 50x50 to 500x500 are used to collect reasonable statistics for the case of isotropic models. The minimum number of realizations necessary for each system size was obtained by conducting the sensitivity analysis on the calculated percolation threshold. For a given system size, the minimum number of realizations is considered the point above which there is no significant change, as shown in Figure 4. Moreover, a summary for the minimum number of realizations and the apparent percolation threshold values (defined as the inflection point on the percolation probability curve in Figure 20) for various system sizes are summarized in Table 4.

For checking the reliability of the code, the average percolation probability values are calculated at various system sizes and their corresponding standard deviations.

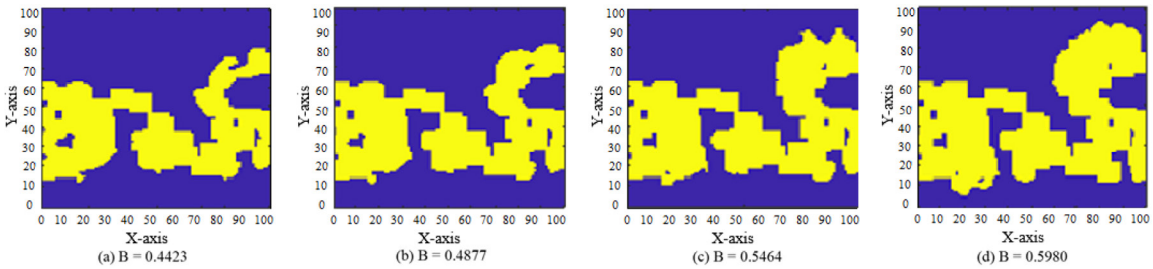

Fig. 3 The patterns of backbone fraction for the realization shown in Figure 2 (e) are obtained by considering the four different flow thresholds. Figures (a), (b), (c) and (d) correspond to the flow thresholds 1 to 4, listed in Table 2, respectively—a smaller flow threshold results in a larger backbone fraction.

Table 3 The description of models used to build anisotropic systems.

No.	System sizes ($x \times y$)	Aspect ratio ω	No.	System sizes ($x \times y$)	Aspect ratio ω
1	100×50	2	6	100×25	4
2	100×75	2	7	100×37.5	4
3	100×100	2	8	100×50	4
4	100×150	2	9	100×75	4
5	100×250	2	10	100×125	4

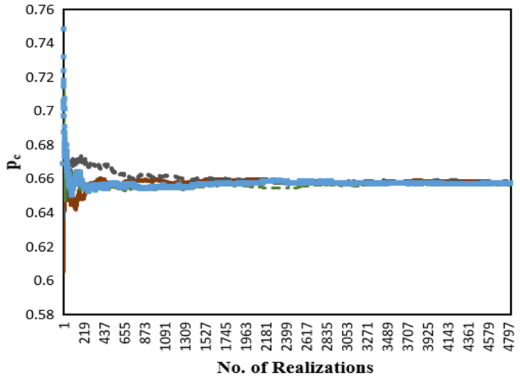

Fig. 4 Sensitivity analysis on the calculated percolation threshold for isotropic models, for example, for a system size =300×300.

Table 4 The estimated values for the apparent percolation threshold and the minimum number of realizations for the isotropic models.

System size ($x \times y$)	Minimum number of realizations	Apparent percolation threshold
500×500	50	0.658
300×300	250	0.653
200×200	400	0.649
150×150	650	0.644
100×100	1250	0.633
50×50	2500	0.614

After that, the curves were rescaled using finite-size scaling (Equation 8). Then, the results are compared with those reported in the literature [2,4, 20]. As an illustrative example, the results of the average percolation probabilities in both original value and rescaled form are shown in Figure 5, in agreement with the previous publications [2, 4, 23, 28, 31]. Moreover, Equation 4 was used for the calculation of apparent percolation thresholds at various system sizes that gives the following size dependency for isotropic models,

$$\tilde{p}_c = -0.1785 \times L^{-0.75} + 0.6674 \quad (13)$$

As mentioned before, a flow-based approach was used to determine the backbone and dead ends fractions. However, to do this correctly, it is needed to set a minimum flow threshold. To determine a suitable threshold, the amount of flow that passes through each grid, the total fluid flow through the whole medium (Q_T) as well as the flow which passed through the backbone structure (Q_B) are determined. Moreover, suitable criteria which result in a minimum difference between the amount of flow through the whole medium and the amount of flow through the backbone structure are needed. In Figure 6, the results of differences in the Q_B and Q_T are shown. As can be seen, the threshold no. 3 (Table 2) may be selected as the best indicator for recognizing the backbone fraction. Thresholds no. 1 and no. 2 resulted in a relatively high difference between the flow in the backbone and the total flow. On the other hand, threshold no. 4 is very small and has almost no effect. Hence, using threshold no. 3, the backbone and dangling end fractions at various system sizes and for all realizations are determined. Figures 7 and 8 show the results for the magnitude of the backbone and dangling ends fractions and their associated uncertainties (i.e. standard deviation values).

Scaling transformation has then been applied to the dataset shown in Figures 9 and 10 to obtain the master curves for the backbone and dangling ends fractions of isotropic systems. In the literature, two values are reported for β_B, 0.478 and 0.63 [4,29]. Furthermore, β_D is reported as -0.423 and -0.23 [4,29]. However, it has been numerically found that these values cannot satisfy finite-size scaling for the simulated dataset. In this study, similar scaling (Equations 6-7 and Equations 9-10) was used to determine the numerical values of the critical exponents β_B and β_D. The estimated values for β_B and β_D were found to be in the range of 0.3 to 0.45] and -0.45 to -0.20, respectively, in line with reported values in the literature [4,29]. These exponent values were used to get the data collapse and determine the master curves. Figures 9 and 10 show the results of the rescaling for the backbone and dangling ends fractions of isotropic models, respectively.

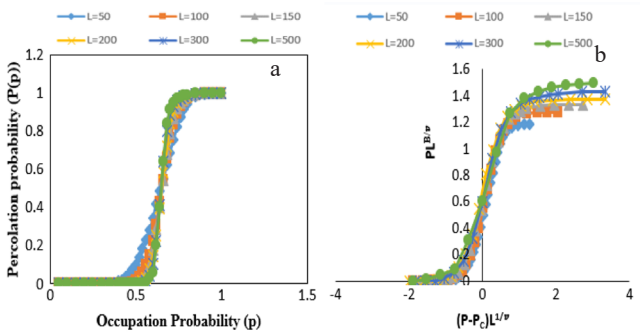

Fig. 5 The plot of the average percolation probability at different system sizes of isotropic models in (a) usual form (b) rescaled form using finite scaling law.

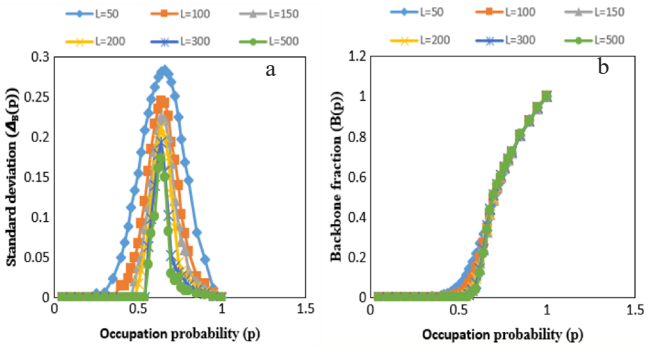

Fig. 7 Illustration of the results of Backbone fraction for isotropic models (a) average value and (b) standard deviation.

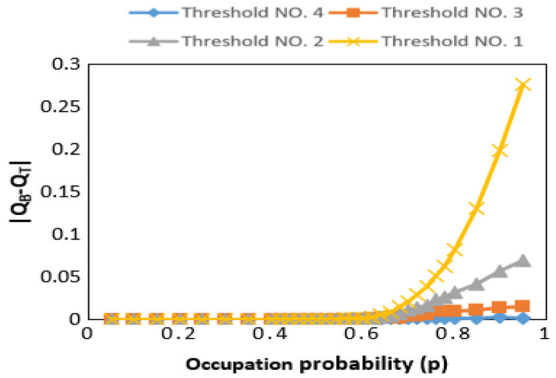

Fig. 6 Sensitivity analysis on the total fluid flow (Q_T) and the flow which passed through the backbone (Q_B) for different values of the minimum flow threshold listed in Table 2.

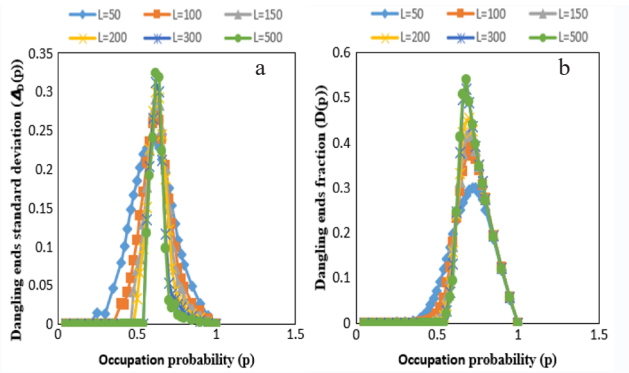

Fig. 8 Illustration of the results of Dangling ends fraction for isotropic models (a) average value and (b) standard deviation.

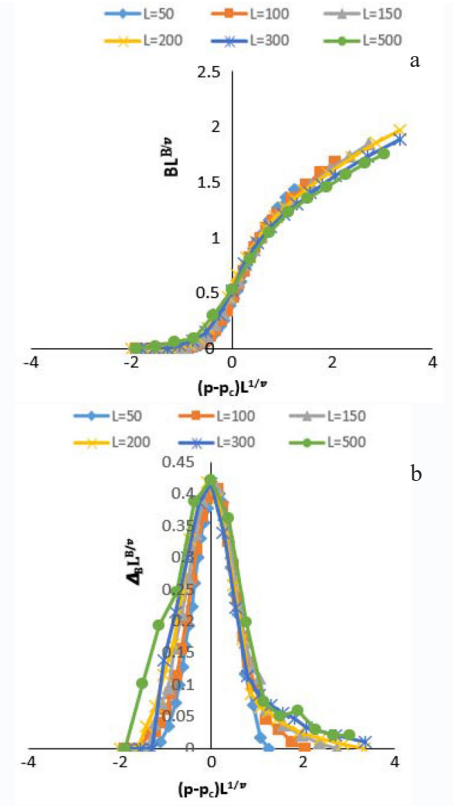

Fig. 9 Finite-size scaling of randomly spatially distributed sand bodies for different isotropic system sizes (a) backbone fraction and (b) the standard deviation of the backbone fraction.

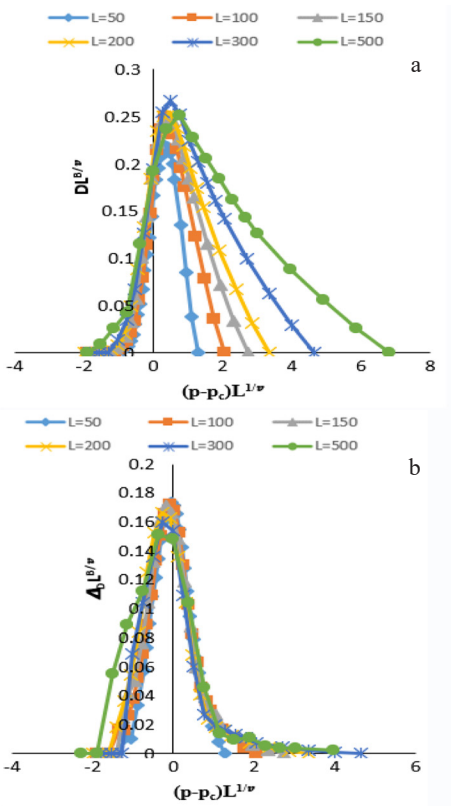

Fig. 10 Finite-size scaling of randomly spatially distributed sand bodies for different isotropic system sizes (a) dangling ends fraction and (b) the standard deviation of the dangling ends fraction.

Anisotropic Sandbody Models

Again, for anisotropic systems described in Table 3, it is first needed to numerically determine the minimum number of realizations for which the simulation results become statistically reasonable. In Table 5, the results of the sensitivity analysis on the percolation threshold to determine the minimum number of realizations for the case of anisotropic models are shown. It indicates that the percolation threshold will increase as effective length or aspect ratio increase. In addition, the percolation threshold in the X direction is higher than the threshold in the Y direction because the effective length in the X direction is larger. For anisotropic systems, the thresholds have been defined as an occupancy probability that more than 50% of realizations are connected [2].

Table 5 Apparent threshold in the X and Y direction and minimum number of realizations as a result of sensitivity analysis for the anisotropic models.

	Effective length, $L_{eff,X}$	Aspect ratio, ω	Minimum number of realizations	Pc in the X direction	Pc in the Y direction
1	10	2	2000	0.716	0.618
2	15	2	1600	0.703	0.631
3	20	2	1200	0.696	0.638
4	30	2	700	0.688	0.645
5	50	2	200	0.681	0.652
6	10	4	3000	0.821	0.512
7	15	4	2500	0.781	0.553
8	20	4	2000	0.758	0.575
9	30	4	1600	0.781	0.553
10	50	4	850	0.821	0.512

Figures 11 and 12 show the results of percolation probability and its associated standard deviation in the X and Y directions for anisotropic systems with aspect ratios ω=2 and 4 as listed in Table 5. As shown in these figures, the direction with the smallest effective length in an anisotropic system has the highest value of percolation probability. The percolation probability itself has a minimum standard deviation under such circumstances. Also, percolation probability determined from each system size behaves differently. Similarly, Figures 13 to 16 show the results for backbone and dangling ends fractions and their associated standard deviations for anisotropic models with aspects values of ω=2 and 4. These results also clearly indicate the dependency of the percolation property on the system size and the separation of the percolation property curves obtained for the x and y directions compared to the isotropic case.

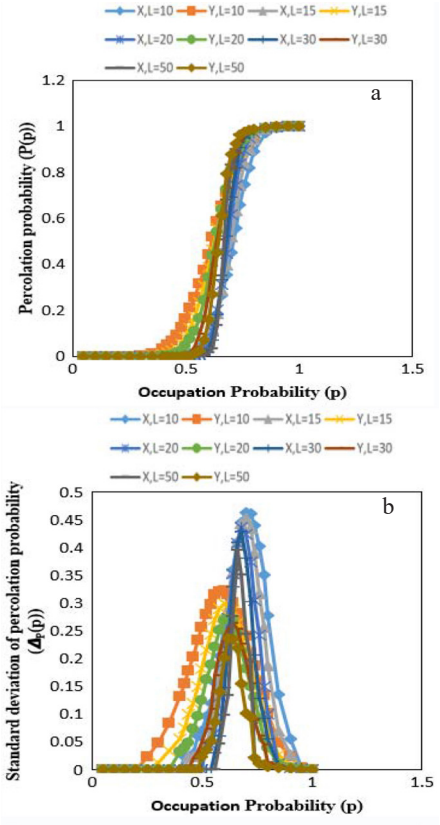

Fig. 11 (a) Percolation probability and (b) its associated standard deviation of anisotropic models with ω=2 for system sizes listed in Table 5.

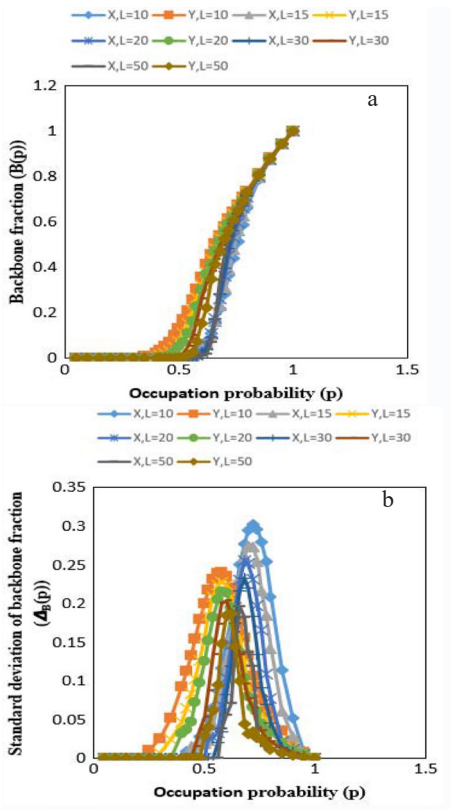

Fig. 13 (a) Backbone fraction and (b) its associated standard deviation of anisotropic models with ω=2 for system sizes listed in Table 5.

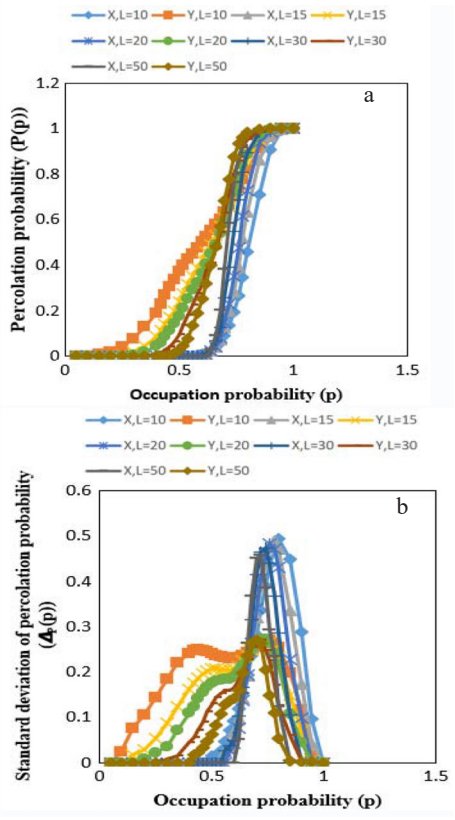

Fig. 12 (a) Percolation probability and (b) its associated standard deviation of anisotropic models with ω=4 for system sizes listed in Table 5.

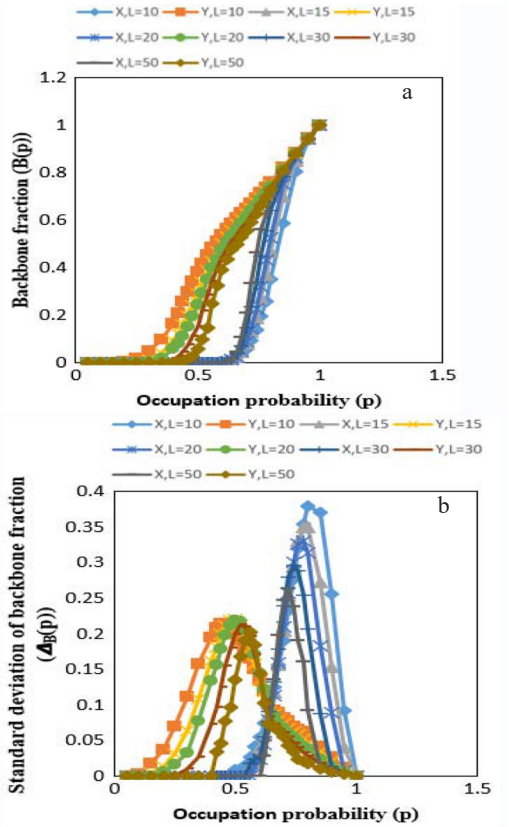

Fig. 14 (a) Backbone fraction and (b) its associated standard deviation of anisotropic models with ω=4 for system sizes listed in Table 5.

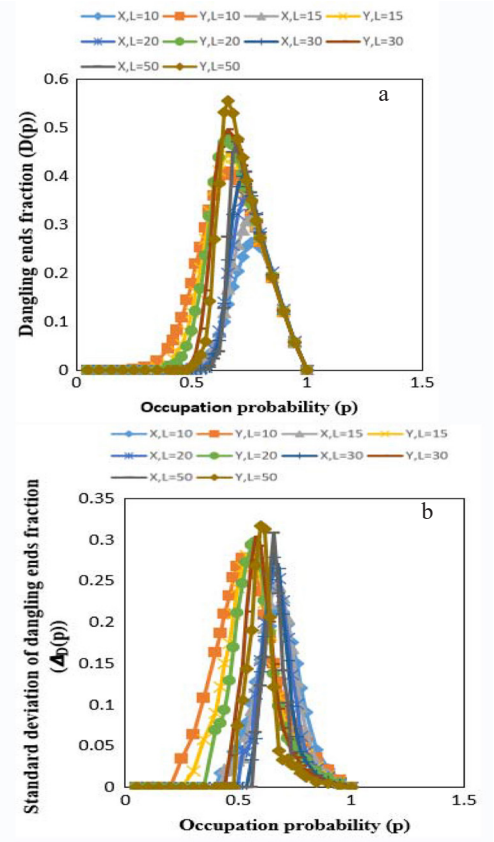

Fig. 15 (a) Dangling ends fraction and (b) its associated standard deviation of anisotropic models with ω=2 for system sizes listed in Table 5.

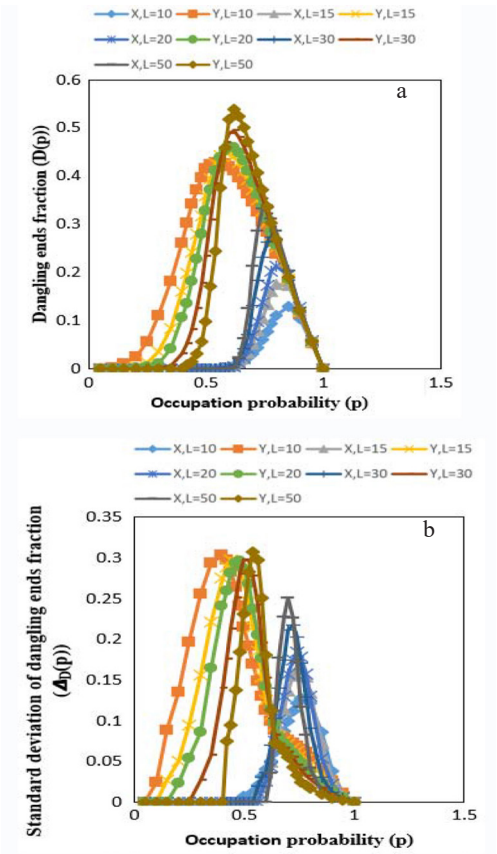

Fig. 16 (a) Dangling ends fraction and (b) its associated standard deviation of anisotropic models with ω=4 for system sizes listed in Table 5.

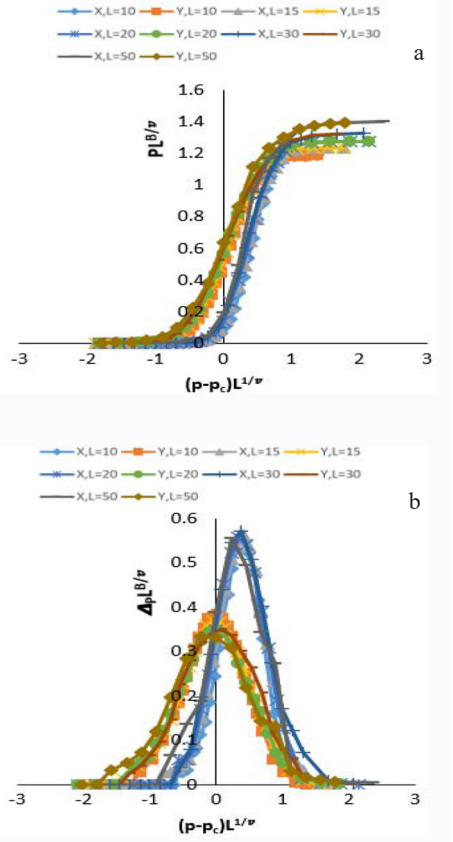

Fig. 17 Finite-size scaling for anisotropic systems of different effective length sizes is listed in Table 5 with ω=2, (a) percolation probability and (b) its associated standard deviation.

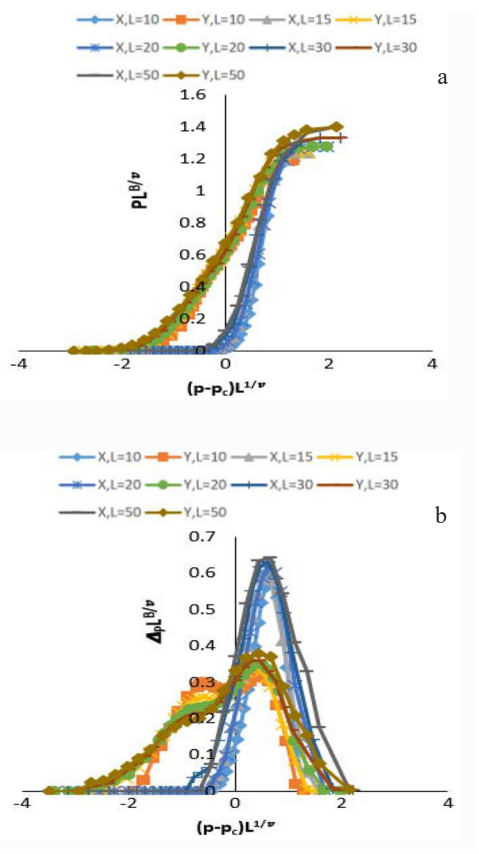

Fig. 18 Finite-size scaling for anisotropic systems of different effective length sizes is listed in Table 5 with ω=4, (a) percolation probability and (b) its associated standard deviation. The percolation threshold of the infinite system is used to obtain scaling curves.

Figures 17 and 18 show the results of finite-size scaling for the percolation probability; moreover, P of anisotropic systems (ω=2 and ω=4) is obtained by using the infinite percolation threshold. As emphasized earlier, using infinite percolation threshold in scaling Equations 5 to 8, for example, for the average percolation probability (in the x and y directions), cannot collapse the percolation probability results. However, suppose the apparent threshold introduced in Equation 13 is used instead of the infinite percolation threshold, as suggested by King and Masihi in 2018 [4]. In that case, the percolation probability curves of the x and y directions will collapse on top of each other. Figures 19 and 20 show these data collapse results. The comparison of the quality of data collapse in Figures 19 and 20 show that the ability of the proposed approach to get data collapse become weak as the anisotropy of the system become stronger.

Furthermore, the scaling curves for the results of the backbones and dangling ends fractions and their associated standard deviations using the proposed apparent threshold in Equation 13 are shown in Figures 21 to 24. Again, these results show the potential of the proposed approach to rescale the percolation properties obtained in each direction and collapse them on each other and the results of the isotropic case. Moreover, comparison of the results in Figures 21 and 22 or Figures 23 and 24 indicate that the quality of collapse data depends on the level of anisotropy and get a weak data collapse as the anisotropy of the system becomes stronger.

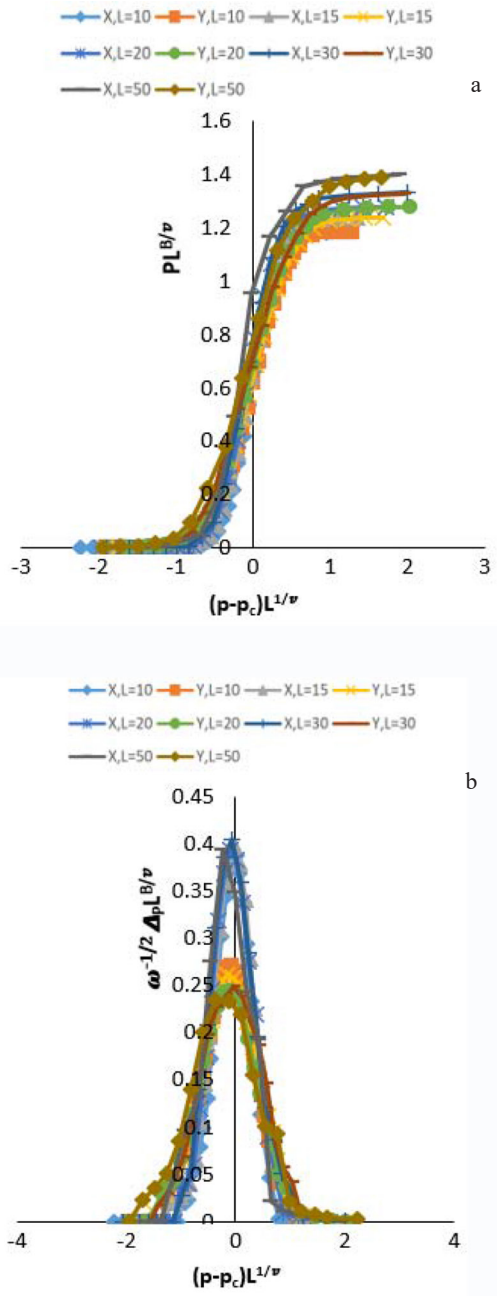

Fig. 19 Finite-size scaling for anisotropic systems of different effective length sizes is listed in Table 5 with ω=2, (a) percolation probability and (b) its associated standard deviation. An apparent percolation threshold is used to obtain scaling curves.

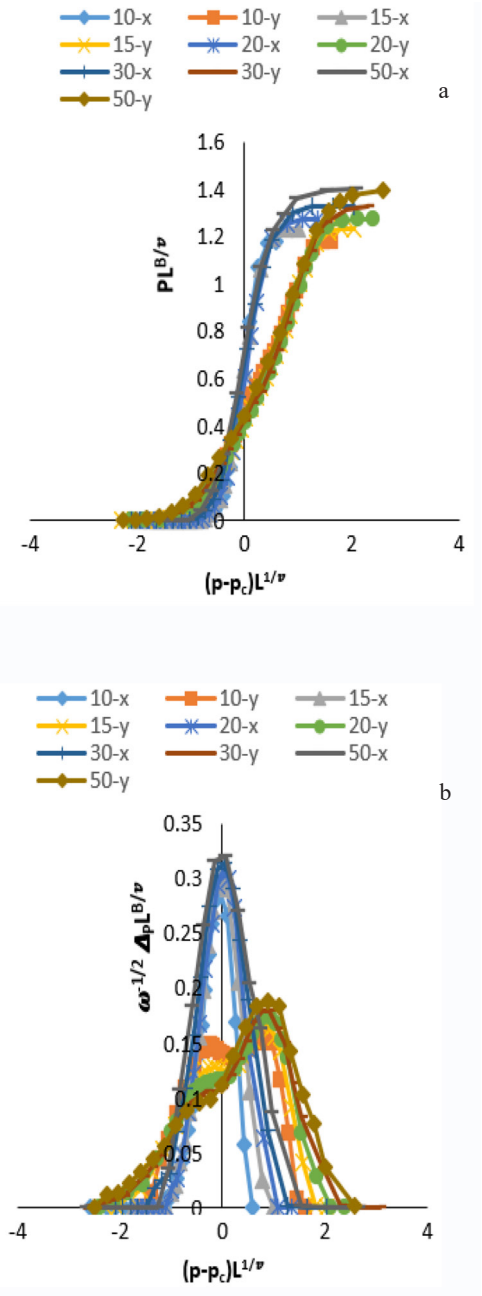

Fig. 20 Finite-size scaling for anisotropic systems of different effective length sizes is listed in Table 5 with ω=4, (a) percolation probability and (b) its associated standard deviation. An apparent percolation threshold is used to obtain scaling curves.

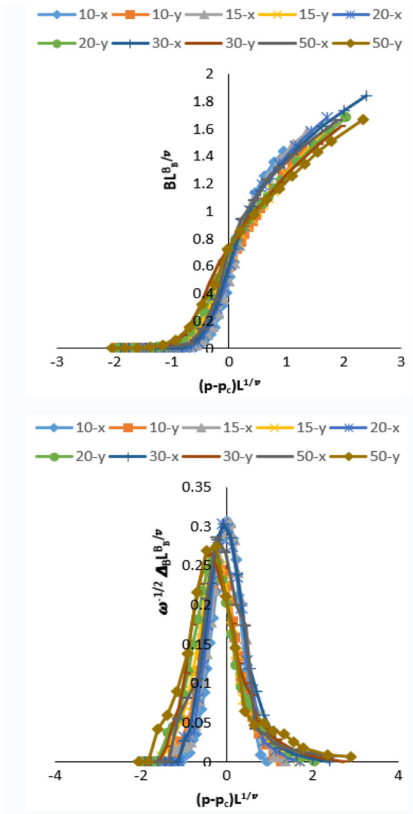

Fig. 21 Finite-size scaling for anisotropic systems of different effective length sizes is listed in Table 5 with ω=2, (a) Backbone fraction and (b) its associated standard deviation. An apparent percolation threshold is used to obtain scaling curves.

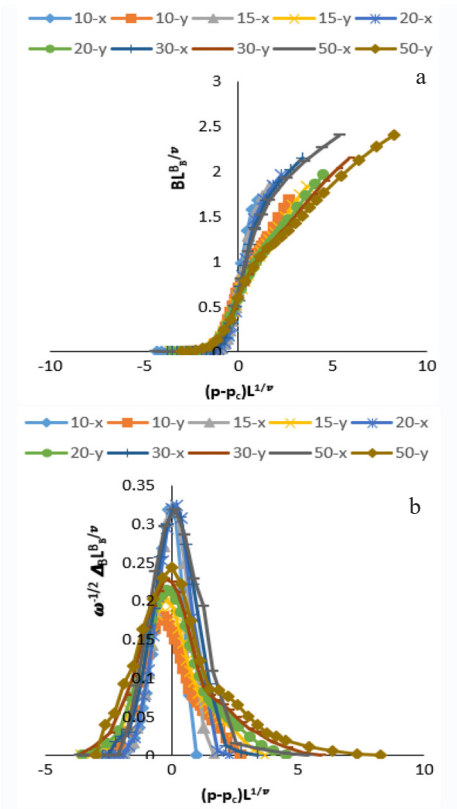

Fig. 22 Finite-size scaling for anisotropic systems of different effective length sizes is listed in Table 5 with ω=4, (a) Backbone fraction and (b) its associated standard deviation. An apparent percolation threshold is used to obtain scaling curves.

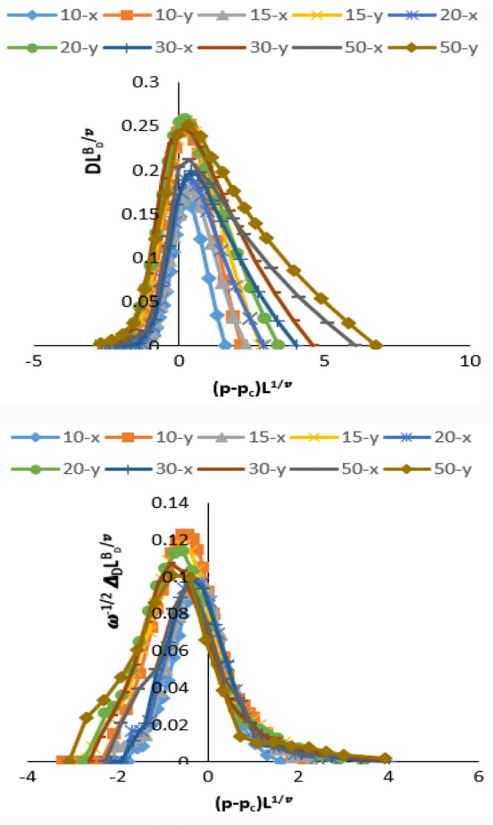

Fig. 23 Finite-size scaling for anisotropic systems of different effective length sizes is listed in Table 5 with ω=2, (a) dangling ends fraction and (b) its associated standard deviation. An apparent percolation threshold is used to obtain scaling curves.

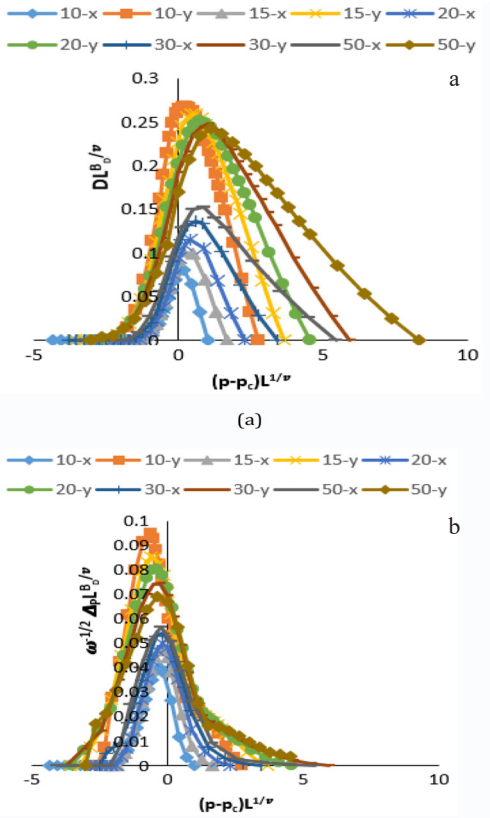

Fig. 24 Finite-size scaling for anisotropic systems of different effective length sizes is listed in Table 5 with ω=4, (a) dangling ends fraction and (b) its associated standard deviation. An apparent percolation threshold is used to obtain scaling curves.

Implementations to Field Data

It is notified that predicting the behavior of the backbones and dangling ends fractions' curves plays a vital role in analysis of flow carrying part of porous media in many applications such as water or chemical flooding in oil reservoirs and water injection on geothermal reservoirs. To apply this approach to real reservoirs, the limitations of this approach must be considered. First, the reservoir model must be a binary type consisting non reservoir (non permeable) and reservoir (permeable) rock types. Second, the connectivity between these reservoir and non-reservoir rock types is the main one that controls the flow behavior in the medium. Other factors such as fluid properties are not critical.

To implement the percolation approach, first, it is needed to transform the reservoir model to become percolation type reservoir (i.e. binary medium). This can be done by setting a threshold value on, for example, reservoir permeability probability distribution. Below this threshold, all reservoir gridblocks are considered non-reservoir and above-considered reservoir parts with a fixed permeability for all grid blocks. Afterwards, a conventional flow simulator with appropriate input data and constraints can be run for a well-pair considered in such a reservoir. This will give the amount of connected oil between two wells and the amount of oil non connected between the wells, which can then be compared with the predictions provided by each of the type curves (Figures 22-25). Applying this approach to some real anisotropic reservoirs and performing sensitivity analysis to answer the reasonable value for permeability threshold or the correct permeability for grid blocks considered reservoir parts is the objective of the future work.

In addition, to estimate the sweep efficiency in oil reservoirs, the results of this study enable us to estimate the volume of water that can be in touch in geothermal reservoirs to transfer heat from the reservoir to the injected water, or to determinethe fluid flow paths in the flooding process in the reservoirs which helps process optimization.

Conclusions

The percolation sub-networks of overlapping sand bodies have been analyzed in this research work. In reservoir engineering applications, these are the amount of oil non-connected to a pair injection and production wells and the fraction of connected oil recoverable. In particular, isotropic and anisotropic percolation type reservoir models in two dimensions were built by considering permeable sand bodies randomly distributed in non-permeable backgrounds with different effective lengths. Then, the behavior of the backbone and dangling end fractions of anisotropic sand bodies representing the recoverable oil connected between two wells and remaining unswept oil and their associated uncertainties were investigated. Provided a considerable simulation studies on the generated models, we first apply scaling equations from percolation theory to estimate the model parameters such as percolation threshold and the critical exponents for power-law scaling equations for isotropic cases. It results in a range for the critical exponents for the backbone and dangling end fractions that are 0.3, 0.45 and -0.45, -0.20, respectively, which were consistent with previous publications on the critical exponent of backbone and provided a new range for the critical exponent of dangling ends. Then, the appropriate forms of the scaling curves in the case of anisotropic models were investigated. The results showed that the percolation properties in the x and y directions get displaced from the isotropic case for the anisotropic models. However, considering the apparent threshold can rescale the percolation properties curves of different directions and put them on the known isotropic percolation properties' curve. A suitable flow criterion that gives the minimum flow to pass each grid cell was used through a sensitivity analysis to distinguish the backbone and dangling ends. The results show that this threshold for the flow through each grid to characterize the backbone fraction depends on the effective length of the system. Using the determined master curves for each percolation property, the backbone from dangling ends fractions can be estimated quickly by a simple algebraic manipulation. This method can be used in the decision-making process, especially in the early development stage of the reservoir when data are very limited, in projects like water flooding or selecting proper positions to drill new wells in anisotropic reservoirs.

References

1. King P R (1990) The connectivity and conductivity of overlapping sand bodies, in North Sea Oil and Gas Reservoirs—II, Springer, 353-362.
2. Sadeghnejad S, Masihi M, King P R, Shojaei A, Pishvaei M (2010) Effect of anisotropy on the scaling of connectivity and conductivity in continuum percolation theory. Physical Review E, 81, 6: 061119.
3. Soltani A, Sadeghnejad S (2018) Scaling and critical behavior of lattice and continuum porous media with different connectivity configurations, Physica A: Statistical Mechanics and its Applications, 508: 376-389.
4. King P R and Masihi M (2018) Percolation theory in reservoir engineering, 1st edition,: world scientific, 1-384.
5. Chattopadhyay P B, Vedanti N (2016) Fractal characters of porous media and flow analysis, in Fractal Solutions for Understanding Complex Systems in Earth Sciences, Springer, 67-77.
6. Hunt A G, Ghanbarian B (2016) Percolation theory for solute transport in porous media: Geochemistry, geomorphology, and carbon cycling, Water Resources Research, 52, 9: 7444-7459..
7. Hunt A, Ewing R, Ghanbarian B (2014) Percolation theory for flow in porous media, Springer, 880: 3319037714.
8. Sahini M, Sahimi M (1994) Applications of percolation theory, 1st edition, CRC Press, 1-276.
9. Broadbent S R, Hammersley J M (1957) Percolation processes: I. Crystals and mazes, Cambridge University Press, 53, 3: 629-641.
10. Stauffer D, Aharony A, Introduction to percolation theory (1992) Taylor and Francis, London, 2nd edittion, 1-192.
11. Berkowitz B, Balberg I (1992) Percolation approach to the problem of hydraulic conductivity in porous media. Transport in Porous Media, 9, 3: 275-286.

12. Berkowitz B (1995) Analysis of fracture network connectivity using percolation theory. Mathematical Geology, 27, 4: 467-483.
13. Rintoul M D, Torquato S (1997) Precise determination of the critical threshold and exponents in a three-dimensional continuum percolation model. Journal of Physics A: Mathematical and General, 30, 16: 305-4470.
14. Hoshen J, Berry M, Minser K (1997) Percolation and cluster structure parameters: The enhanced Hoshen-Kopelman algorithm. Physical Review E, 56, 2: 1455.
15. Dokholyan N V, Lee Y, Buldyrev S V, Havlin S, King P R, Stanley H E (1998) Scaling of the distribution of shortest paths in percolation. Journal of Statistical Physics, 93, 3: 603-613.
16. Berkowitz B, Balberg I (1993) Percolation theory and its application to groundwater hydrology, Water Resources Research, 29, 4: 775-794.
17. Vogel E E, Lebrecht W, Valdés J F (2010) Bond percolation for homogeneous two-dimensional lattices. Physica A: Statistical Mechanics and its Applications, 389, 8: 1512-1520.
18. Lee S B, Torquato S (1990) Monte Carlo study of correlated continuum percolation: Universality and percolation thresholds. Physical Review A, 41, 10: 5338.
19. Lorenz C D, Ziff R M (2001) Precise determination of the critical percolation threshold for the three-dimensional "Swiss cheese" model using a growth algorithm, The Journal of Chemical Physics, 114, 8: 3659-3661.
20. Masihi M, King P R, Nurafza P R (2005) Fast estimation of performance parameters in fractured reservoirs using percolation theory, Society of Petroleum Engineers, OnePetro.
21. Masihi M, King P R (2007) A correlated fracture network: modeling and percolation properties, Water Resources Research, 43, 7: 0043-1397.
22. Masihi M, King P R, Nurafza P R (2008) Connectivity prediction in fractured reservoirs with variable fracture size: analysis and validation, SPE Journal, 13, 1: 88-98 .
23. Sadeghnejad S, Masihi M, King P R, Shojaei A, Pishvaie M (2011) A reservoir conductivity evaluation using percolation theory, Petroleum Science and Technology, 29, 10: 1041-1053
24. Sadeghnejad S, Masihi M, Pishvaie M, King P R (2013) Rock type connectivity estimation using percolation theory, Mathematical Geosciences, 45, 3: 321-340.
25. Tavagh-Mohammadi B, Masihi M, Ganjeh-Ghazvini M (2016) Point-to-point connectivity prediction in porous media using percolation theory. Physica A: Statistical Mechanics and its Applications, 460: 304-313.
26. Sadeghnejad S, Masihi M (2016) Point to point continuum percolation in two dimensions. Journal of Statistical Mechanics: Theory and Experiment, 10: 103210.
27. King P R, Buldyrev S V, Dokholyan N V, Havlin S, Lee Y, Paul, G., Stanley, H.E. Vandesteeg N (2001) Predicting oil recovery using percolation theory. Petroleum Geoscience, 7: 105-107.
28. Nurafza P R, King P R, Masihi M (2006) Facies connectivity modelling: analysis and field study, Society of Petroleum Engineers, OnePetro.
29. Wen H, King P R, Muggeridge A H, Vittoratos E S (2014) Using percolation theory to estimate recovery from poorly connected sands using pressure depletion, In ECMOR XIV-14th European Conference on the Mathematics of Oil Recovery, European Association of Geoscientists and Engineers, 1-13..
30. Hoshen J, Berry M W, Minser K S (1997) Percolation and cluster structure parameters: The enhanced Hoshen-Kopelman algorithm. Physical Review E, 56, 2: 1455.
31. Nurafza P R, King P R, Masihi M (2006) Connectivity modeling of heterogeneous systems: analysis and field study, Computational Methods in Water Resources, 19-22..